STRUCTURAL BIOLOGY COMMUNICATIONS

ISSN 2053-230X

Crystal structure of 5-enolpyruvylshikimate-3-phosphate (EPSP) synthase from the ESKAPE pathogen *Acinetobacter baumannii*

Kristin A. Sutton,[a]‡ Jennifer Breen,[a] Thomas A. Russo,[b,c] L. Wayne Schultz[a,d]§ and Timothy C. Umland[a,d]*§

[a]Hauptman–Woodward Medical Research Institute, Buffalo, NY 14203, USA, [b]Department of Medicine and The Witebsky Center for Microbial Pathogenesis, University at Buffalo, State University of New York, Buffalo, NY 14214, USA, [c]Veterans Administration Western New York Healthcare System and Department of Microbiology and Immunology, University at Buffalo, State University of New York, Buffalo, NY 14214, USA, and [d]Department of Structural Biology, University at Buffalo, State University of New York, Buffalo, NY 14203, USA. *Correspondence e-mail: umland@hwi.buffalo.edu

Received 15 December 2015
Accepted 19 January 2016

Edited by T. C. Terwilliger, Los Alamos National Laboratory, USA

‡ Present address: HarkerBIO, Buffalo, NY 14203, USA.
§ Present address: QuaDPharma, Clarence, NY 14031, USA.

Keywords: shikimate pathway; *Acinetobacter baumannii*; essential genes; antibiotic targets; multidrug resistance; EPSP synthase.

PDB reference: EPSP synthase from *A. baumannii*, 5buf

Supporting information: this article has supporting information at journals.iucr.org/f

The enzyme 5-enolpyruvylshikimate-3-phosphate (EPSP) synthase catalyzes the sixth step of the seven-step shikimate pathway. Chorismate, the product of the pathway, is a precursor for the biosynthesis of aromatic amino acids, siderophores and metabolites such as folate, ubiquinone and vitamin K. The shikimate pathway is present in bacteria, fungi, algae, plants and apicomplexan parasites, but is absent in humans. The EPSP synthase enzyme produces 5-enolpyruvylshikimate 3-phosphate and phosphate from phosphoenolpyruvate and shikimate 3-phosphate *via* a transferase reaction, and is the target of the herbicide glyphosate. The *Acinetobacter baumannii* gene encoding EPSP synthase, *aroA*, has previously been demonstrated to be essential during host infection for the growth and survival of this clinically important drug-resistant ESKAPE pathogen. Prephenate dehydrogenase is also encoded by the bifunctional *A. baumannii aroA* gene, but its activity is dependent upon EPSP synthase since it operates downstream of the shikimate pathway. As part of an effort to evaluate new antimicrobial targets, recombinant *A. baumannii* EPSP ($_{Ab}$EPSP) synthase, comprising residues Ala301–Gln756 of the *aroA* gene product, was overexpressed in *Escherichia coli*, purified and crystallized. The crystal structure, determined to 2.37 Å resolution, is described in the context of a potential antimicrobial target and in comparison to EPSP synthases that are resistant or sensitive to the herbicide glyphosate.

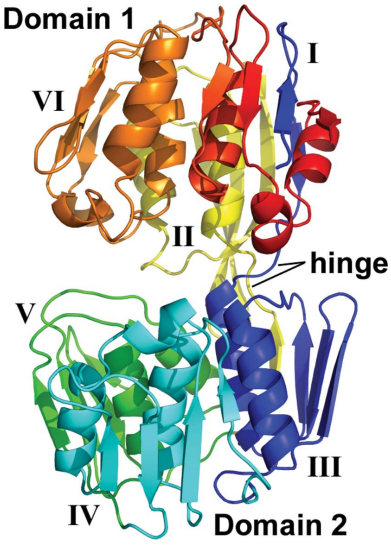

1. Introduction

Infections owing to drug-resistant *Acinetobacter baumannii* are becoming increasingly commonplace, with resultant increases in morbidity, mortality and healthcare-associated costs (Spellberg & Bonomo, 2014; Villar *et al.*, 2014). The Centers for Disease Control and Prevention (CDC) has designated the threat level for *A. baumannii* as serious (Centers for Disease Control and Prevention, 2013), and it has been included as an ESKAPE pathogen to emphasize the threat to public health (Boucher *et al.*, 2013; Paterson & Harris, 2015). Recently, up to 50% of *A. baumannii* isolates were classified as extensively drug-resistant (XDR) in US intensive-care units (Lee *et al.*, 2014; Spellberg & Bonomo, 2014). The promise of a post-antibiotic era is on the cusp of being fulfilled by *A. baumannii* (Garnacho-Montero & Amaya-Villar, 2010; Kim *et al.*, 2009; Napier *et al.*, 2013; Perez *et al.*, 2007) and true pan-drug-resistant (PDR) strains have been reported (Göttig *et al.*, 2014; Rolain *et al.*, 2013). Therefore, our group has focused on the identification and

validation of new or underexploited antimicrobial targets within *A. baumannii* (Russo *et al.*, 2009, 2010; Umland *et al.*, 2012, 2014). An efficient genetic screen was developed to identify *A. baumannii* genes that are essential *in vivo* (*i.e.* essential for pathogen growth and survival in an infected host; Umland *et al.*, 2012). The resulting gene set identified by this *in vivo* essentiality screen included two *A. baumannii* shikimate-pathway genes: *aroA* [encoding 5-enolpyruvylshikimate-3-phosphate (EPSP) synthase] and *aroC* (encoding chorismate synthase). The *A. baumannii aroA* gene atypically encodes prephenate dehydrogenase (PD) activity in addition to EPSP synthase, producing a PD-EPSP synthase fusion (Adams *et al.*, 2008). In most prokaryotes, separate enzymes perform these two activities. PD activity is utilized downstream of the shikimate pathway for the biosynthesis of tyrosine. Thus, PD activity is expected to be dependent upon the presence of an intact shikimate pathway. A third *A. baumannii* gene in the shikimate pathway, *aroK* (encoding shikimate kinase), has also been demonstrated to be essential *in vivo* (Sutton *et al.*, 2015), further demonstrating the importance of this metabolic pathway during infection.

The shikimate pathway is present in bacteria, fungi, apicomplexan parasites and plants, with the product chorismate serving as a precursor of aromatic amino acids and other aromatic metabolites, including folate, ubiquinone and vitamin K (Abell, 1999; Bentley & Haslam, 1990; Haslam, 1974; Herrmann & Weaver, 1999; McConkey *et al.*, 2004). Moreover, a number of important bacterial pathogens utilize chorismate-derived siderophores as virulence factors (Miethke & Marahiel, 2007). Inhibition of EPSP synthase (also referred to as 3-phosphoshikimate-1-carboxyvinyl transferase; PSCVT) is the basis of the widely used herbicide glyphosate. The EPSP synthases have been divided into two classes according to intrinsic glyphosate sensitivity (Franz *et al.*, 1997; Funke *et al.*, 2006; Stallings *et al.*, 1991). Class I EPSP synthases, which are present in plants and some bacteria (*e.g.* *Salmonella typhimurium* and *Escherichia coli*), are inhibited at low concentrations of glyphosate. Class II EPSP synthases, which are present in many bacterial species, are glyphosate-resistant. Examples of species possessing the class II enzyme include *Staphylococcus aureus*, *Streptococcus pneumoniae* and, notably, *Agrobacterium* sp. strain CP4. The ortholog from this latter species was used to create commercial transgenic glyphosate-resistant crops (Padgette *et al.*, 1995).

EPSP synthase (EC 2.5.1.19) catalyzes the transfer of the enolpyruvyl moiety of phosphoenolpyruvate (PEP) to the 5-hydroxy position of shikimate 3-phosphate (S3P; Bentley & Haslam, 1990; Levin & Sprinson, 1964), a requisite step in the biosynthesis of chorismate and ultimately aromatic metabolites. The *in vivo* essentiality of *A. baumannii aroA* is at least in part attributed to the EPSP synthase fragment (residues 301–756), as there is no known enzyme substitute or other route to the synthesis of 5-enolpyruvylshikimate 3-phosphate. This pathway is absent from humans, an attractive feature for novel antimicrobial targets (Coggins *et al.*, 2003). However, the respective *A. baumannii* pathway enzymes have not been specifically characterized and validated as antimicrobial targets. Here, the expression, purification, crystallization and structure analysis of unliganded recombinant *A. baumannii* EPSP ($_{Ab}$EPSP) synthase is reported.

Table 1
X-ray data-collection and refinement statistics.

Values in parentheses are for the highest resolution shell.

PDB code	5buf
Data collection	
Space group	$P2_12_12_1$
Unit-cell parameters (Å)	a = 73.9, b = 103.4, c = 113.2
Completeness (%)	96.9 (99.0)
Resolution range (Å)	34.79–2.37 (2.41–2.37)
Total No. of reflections	261575
No. of unique reflections	34884 (1759)
Multiplicity	7.5 (6.3)
R_{meas}	0.080 (0.42)
$\langle I/\sigma(I)\rangle$	17.5 (4.7)
Wilson B factor (Å^2)	28.9
Refinement	
Resolution range (Å)	4.79–2.37 (2.44–2.37)
Completeness (%)	97.0 (99.0)
No. of reflections, working set	33045
No. of reflections, test set	1748
R_{cryst}/R_{free}	0.1833 (0.2103)/0.2285 (0.2518)
No. of non-H atoms	
Protein	6572
Ion	64
Water	423
Model geometry (r.m.s. deviations from ideal)	
Bonds (Å)	0.004
Angles (°)	0.83
Average B factors (Å^2)	
Protein	36.2
Ion	39.0
Water	33.0
Ramachandran plot† (%)	
Favored	98.0
Allowed	1.2
Outliers	0.34
MolProbity clashscore†	0.53
Rotamer outliers† (%)	0.72

† As calculated by *MolProbity*; *MolProbity* clashscore corresponds to the 100th percentile (*i.e.* the best) among structures of comparable resolution.

2. Materials and methods

2.1. Cloning, expression and purification of $_{Ab}$EPSP synthase

Primers (sense, 5′-CGCCCGCATATGAATAAGGTGACACA-3′; antisense, 5′-CGAACGGCTCGAGTTATTGGCTAACT-3′) were synthesized (Integrated DNA Technologies, Iowa, USA) and used to amplify *via* PCR the fragment of the *A. baumannii* strain 307-0294 *aroA* gene (ABBFA_001168) encoding EPSP synthase activity (corresponding to amino-acid residues Ala301–Gln756 of the transcribed gene product; Adams *et al.*, 2008). The PCR product was digested with NdeI and XhoI restriction enzymes and ligated onto the customized expression vector pET-duet-SUMO (Sutton *et al.*, 2015) to construct pET-SUMO-$_{Ab}$EPSPS. The expression-cassette sequence was verified by DNA sequencing (Roswell Park Cancer Institute Sequencing Facility, New York, USA).

Overexpression of $_{Ab}$EPSP synthase occurred in *E. coli* Rosetta (DE3) cells grown in LB medium with 100 µg ml^{-1} ampicillin and 34 µg ml^{-1} chloramphenicol to an OD$_{600}$ of 0.8

at 37°C and then induced with 1 m*M* IPTG and incubated for 4 h. The protein was purified from the crude lysate. The cells were resuspended in lysis buffer consisting of 25 m*M* HEPES pH 7.5, 250 m*M* NaCl, 20 m*M* imidazole, 1 m*M* β-mercaptoethanol (BME) and were lysed using sonication and a Microfluidizer processor (Microfluidics, Massachusetts, USA). The supernatant was loaded onto an immobilized metal ion-affinity chromatography (IMAC) column (HiTrap, GE Healthcare Life Sciences, Pennsylvania, USA). The His_6-SUMO-$_{Ab}$EPSP synthase construct was eluted in 25 m*M* HEPES pH 7.5, 250 m*M* NaCl, 1 m*M* BME with a linear imidazole gradient from 60 m*M* to 1 *M* over 100 ml. The His_6-SUMO tag was cleaved by overnight incubation with Ulp1 protease using a 500:1 mass ratio. The sample was reapplied onto a HiTrap IMAC column to separate the cleaved affinity tag from the $_{Ab}$EPSP synthase. Gel filtration (Superdex 200 HiLoad 16/60; GE Healthcare Life Sciences) was performed as a final step in 25 m*M* HEPES pH 7.5, 250 m*M* NaCl, 1 m*M* dithiothreitol (DTT). Purified $_{Ab}$EPSP synthase was dialyzed into 25 m*M* HEPES pH 8.0, 20 m*M* NaCl, 1 m*M* DTT and then concentrated to 10 mg ml^{-1} (Bradford method) by centrifugal ultrafiltration (YM10 Centricon; EMD Millipore, Massachusetts, USA).

2.2. Crystallization

Crystallization screening *via* microbatch under oil in 1536-multiwell plates was conducted using high-throughput robotics (Luft *et al.*, 2003). Selected crystallization conditions were optimized *via* manual hanging-drop vapor diffusion. The crystals used for diffraction data collection were obtained by equilibration at 293 K of a crystallization drop consisting of 3 µl purified $_{Ab}$EPSP synthase at 10.0 mg ml^{-1} plus 3 µl reservoir solution against 500 µl reservoir solution [100 m*M* bis-tris propane pH 7.0, 100 m*M* potassium bromide, 40%(*w*/*v*) PEG 8000].

2.3. Diffraction data collection and processing

A crystal was harvested using a nylon loop and then flash-cooled in a cryostream at 100 K. Diffraction data were collected using a Saturn 944+ CCD detector and a MicroMax-007 HF copper rotating-anode X-ray source equipped with Osmic Varimax HF optics with a crystal-to-detector distance of 45 mm and 0.5° oscillation and 30 s exposure per frame. The data were integrated and scaled using *HKL*-2000 (Otwinowski & Minor, 1997). *Mycobacterium tuberculosis* EPSP synthase in complex with S3P (PDB entry 2o0b; Mycobacterium Tuberculosis Structural Proteomics Project, unpublished work) was used as the search model for molecular replacement in *MOLREP* (Vagin & Teplyakov, 2010) to generate an initial model. The resulting model was refined using *PHENIX* (Adams *et al.*, 2010), including noncrystallographic symmetry (NCS) torsion-based restraints employing a flexible target function that smoothly shuts off to allow local differences between NCS-related chains. Translation–libration–screw rotation model (TLS) parameter refinement (Afonine *et al.*, 2012) was included at later stages of refinement. Riding H atoms were included during refinement to improve geometry. Iterative manual model building was performed with *Coot* (Emsley *et al.*, 2010). Structure analysis and validation made use of *PyMOL* (Schrödinger), *PHENIX* (Adams *et al.*, 2010), *jsPISA* (Krissinel, 2015) and the validation tools present in the *wwPDB Deposition Tool* (http://deposit.wwpdb.org/deposition). *WebLogo* was used to analyze sequence motifs (Crooks *et al.*, 2004). The refined coordinates and scaled diffraction data have been deposited in the PDB (PDB entry 5buf).

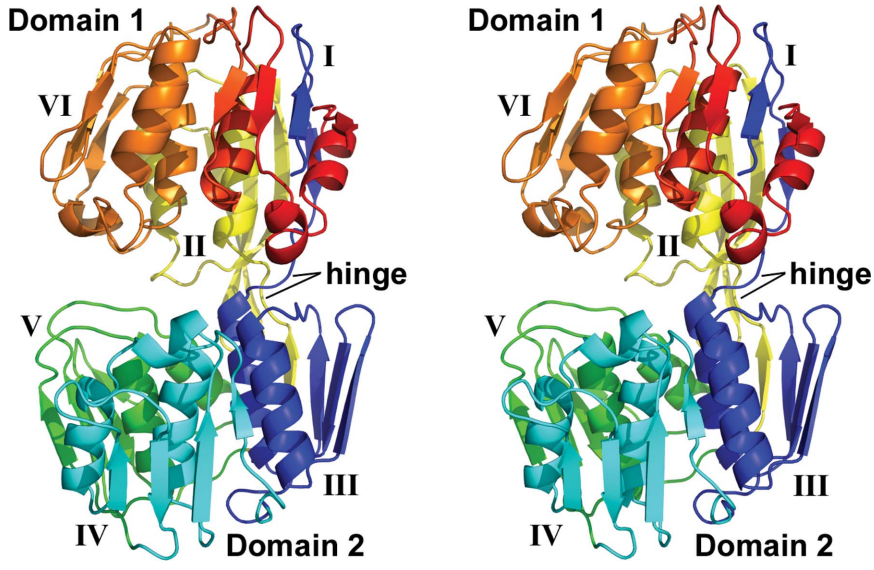

Figure 1
Stereoview of $_{Ab}$EPSP synthase domain organization. The peptide chain is colored sequentially: blue (N-terminus; Thr312–Leu394), cyan (Lys395–Gln468), green (Gln469–Leu537), yellow (Val538–Thr614), orange (Leu615–Gly692) and red (C-terminus; Asp693–Gln756). Individual subdomains are labeled with roman numerals. The N-terminal segment (blue) of the peptide chain participates in the formation of subdomains I, II and III, and a middle segment (yellow) participates in the formation of subdomains II and III. Subdomains IV, V and VI are comprised of contiguous sections of the peptide chain and are colored cyan, green and orange, respectively.

3. Results and discussion

3.1. Overall structure of $_{Ab}$EPSP synthase

Recombinant $_{Ab}$EPSP synthase, comprising amino-acid residues Ala301–Gln756 of the *A. baumannii aroA* gene product, was expressed and purified for crystallization by a three-step chromatography strategy. Diffraction-quality rod-shaped crystals were readily obtained, yielding data to 2.37 Å resolution on a rotating-anode X-ray source (Table 1). Phasing was accomplished by routine molecular replacement using *M. tuberculosis* EPSP synthase as a search model (PDB entry 2o0b; 22% sequence identity), revealing two protomers to be present within the crystallographic asymmetric unit. The sequence corresponding to $_{Ab}$EPSP synthase was built into the initial electron-density map and the subsequent model was refined. Residues Thr312–Gln756 were defined in electron density for both protomers, with the N-terminal residues Ala301–Val311 presumably disordered. The two protomers were structurally similar, with a root-mean-square deviation (r.m.s.d.) of 1.08 Å for aligned C^{α} atoms.

$_{Ab}$EPSP synthase exhibited the twice-repeated domain architecture characteristic of the family. Each domain contains three similar subdomains based upon a $\beta\alpha\beta\alpha\beta\beta$ core architecture, with the two domains connected by a double hinge comprised of residues Thr329–Asp333 and Val544–Asp547. Domain 1 contained subdomains I, II and VI, and domain 2 contained subdomains III, IV and V (Fig. 1), as previously observed (Stallings *et al.*, 1991). Subdomain I contained both the N- and C-termini of the $_{Ab}$EPSP synthase peptide chain owing to the dual crossover between domains. Specifically, the N-terminal residues Gln313–Ile317 form a single β-strand within subdomain I. The remainder of this subdomain is comprised of the C-terminal residues Gly701–Gln756. Likewise, subdomains II and III are formed from a single β-strand

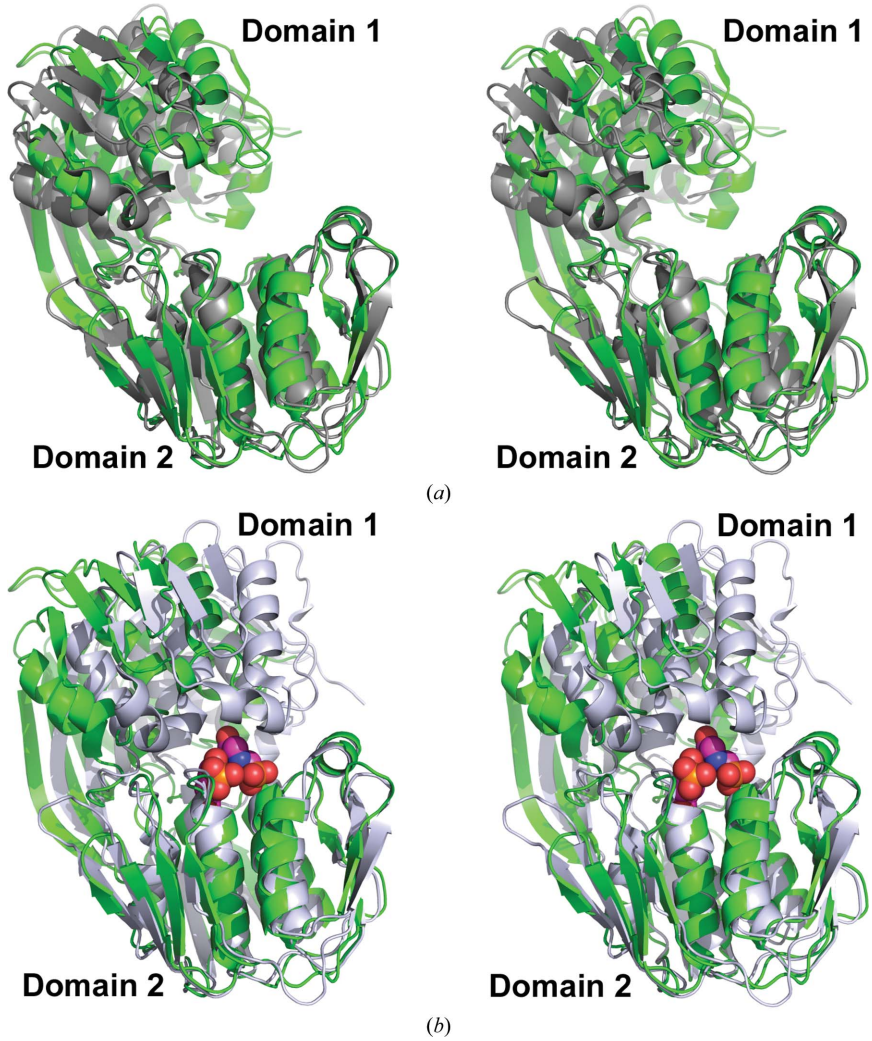

Figure 2
Stereoviews of $_{Ab}$EPSP synthase and $_{CP4}$EPSP synthase superimposed. (*a*, *b*) Cartoon representations of unliganded $_{Ab}$EPSP synthase (green) superimposed upon (*a*) the unliganded, open conformation (PDB entry 2gg4; dark gray) and (*b*) the S3P/glyphosate-bound closed conformation (PDB entry 2gga; gray with ligands displayed as spheres) $_{CP4}$EPSP synthase structures. (*c*, *d*) Predicted ligand-binding residues in $_{Ab}$EPSP synthase (green C atoms) superimposed upon the $_{CP4}$EPSP synthase residues (italicized residue labels) that participate in S3P and PEP/glyphosate binding in (*c*) the unliganded open conformation (PDB entry 2gg4; dark gray C atoms) and (*d*) the S3P/glyphosate-bound closed conformation (PDB entry 2gga; gray C atoms with ligands displayed in ball-and-stick representation with magenta C atoms). In all cases, structures were superimposed using only the C^{α} atoms of domain 2 to emphasize substrate-induced conformational changes. The orientation of $_{Ab}$EPSP synthase is identical in all panels of the figure.

(residues Phe324–Phe328 and Thr540–Val544, respectively) interacting with a discontinuous range of residues (residues Asp547–Gly611 and Asp333–Gly388, respectively) that form the remainder of each subdomain. Subdomains I and IV possess an additional 3_{10}-helix in the connecting residues between the second β-strand and the second α-helix of the core subdomain fold, resulting in a modified $\beta\alpha\beta3_{10}\alpha\beta\beta$ topology. Subdomain VI displays an analogous 3_{10}-helix, which is likely to participate in the transition between the open (unliganded) and closed (substrate-bound) conformations (Funke *et al.*, 2006; Park *et al.*, 2004), plus a second additional helix, to yield a $\beta3_{10}\alpha\beta3_{10}\alpha\beta\beta$ fold. Similar deviations from the core fold have previously been observed in *S. pneumoniae* EPSP ($_{Sp}$EPSP) synthase and *Agrobacterium* sp. strain CP4 EPSP ($_{CP4}$EPSP) synthase (Funke *et al.*, 2006; Park *et al.*, 2004). An approximately twofold-symmetric homodimer was formed by the two $_{Ab}$EPSP synthase protomers present within the crystallographic asymmetric unit. However, the dimer interface only involved subdomain IV (domain 2) and buried only ∼550 Å^2 per protomer. Thus, this dimer was predicted not to be a stable biological assembly using *jsPISA* analysis. Moreover, the protein eluted from a Superdex 200 gel-filtration column as expected for a monomer of 48 kDa. Similarly, the crystallized $_{Sp}$EPSP synthase was observed to form oligomers, but analysis of the solution state indicated only monomers to be present for both unliganded and liganded forms (Park *et al.*, 2004).

3.2. Substrate-induced conformation change

EPSP synthases undergo significant substrate-induced conformational changes upon binding S3P, with complete and productive substrate-binding and active sites formed at the interface between the two domains upon transition to the closed conformation (Funke *et al.*, 2006; Park *et al.*, 2004; Schönbrunn *et al.*, 2001). The $_{Ab}$EPSP synthase structure reported here is in the open conformation, as expected given the absence of bound substrate (Fig. 2*a*). S3P is thought to initially bind to domain 2, triggering the switch to the closed conformation. Superimposing the C$^{\alpha}$ atoms of domain 2 from $_{Ab}$EPSP synthase (unliganded, open conformation) with those of $_{CP4}$EPSP synthase (unliganded, open conformation; PDB

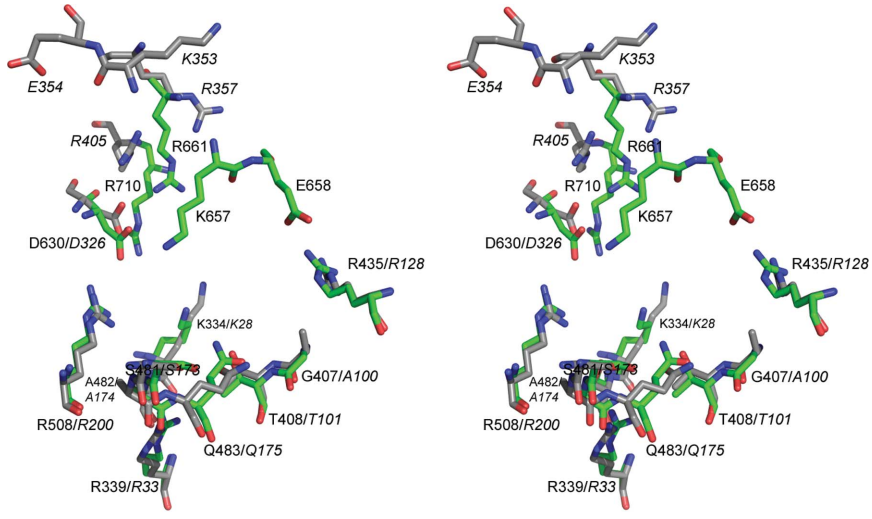

Figure 2 (continued)

entry 2gg4; Funke *et al.*, 2006) and of the $_{CP4}$EPSP synthase–S3P–glyphosate complex (closed conformation; PDB entry 2gga; Funke *et al.*, 2006) resulted in r.m.s.d. values of 1.92 and 1.88 Å, respectively, for aligned C^{α} atoms of domain 2 (Figs. 2*a* and 2*b*). In comparison, the r.m.s.d. was 0.79 Å for the superimposed C^{α} atoms of domain 2 of the two $_{CP4}$EPSP synthase structures. Plotting the set of lines connecting paired atoms of two structurally aligned proteins is useful for evaluating both domain-level and localized conformational differences between two members of the same family (*i.e.* $_{Ab}$EPSP and $_{CP4}$EPSP synthases) or between the same protein in different states (*i.e.* open *versus* closed conformations). The aligned paired-atom lines obtained upon global structural alignments indicated that the largest domain-level conformational differences occur primarily for domain 1 both between EPSP synthase orthologs and between states (Fig. 3*a*). Upon structural alignment of only domain 2, the corresponding paired-atom lines displayed negligible differences within domain 2 both between orthologs and between states (Fig. 3*b*). These analyses suggested that domain 2 is structurally very similar between $_{Ab}$EPSP synthase and $_{CP4}$EPSP synthase and does not undergo major structural changes upon binding S3P and the subsequent conversion from the open to the substrate-bound closed conformation.

Conversely, a similar comparison of superimposed C^{α} atoms of domain 1 demonstrated that domain 1 exhibits greater localized structural diversity both between orthologs and between the open and closed conformations of the same ortholog (Figs. 2*b*, 3*a* and 3*c*). Specifically, superimposing the domain 1 C^{α} atoms of $_{Ab}$EPSP synthase (unliganded, open conformation) on those of $_{CP4}$EPSP synthase (unliganded, open conformation; PDB entry 2gg4) and the $_{CP4}$EPSP synthase–S3P–glyphosate complex (closed conformation; PDB entry 2gga) resulted in r.m.s.d. values of 3.41 and 3.22 Å, respectively, for aligned domain 1 C^{α} atoms. By comparison, the r.m.s.d. was 1.65 Å for superimposed C^{α} atoms of domain 1 of $_{CP4}$EPSP synthase in open and closed conformations. The paired-atom lines for superimposed C^{α} atoms of domain 1 of $_{Ab}$EPSP synthase and open $_{CP4}$EPSP synthase revealed two regions of significant localized differences (Fig. 3*c*). The region distant from the substrate-binding site differed owing to differences in loop structures connecting core secondary-structural elements, and thus is probably functionally unimportant. The second region borders the substrate-binding site and includes $_{Ab}$EPSP synthase residues Thr649–Arg661. Interestingly, these structural differences in domain 1 at the substrate-binding site are largely absent in the alignment of $_{Ab}$EPSP synthase with closed $_{CP4}$EPSP synthase, but are present for open *versus* closed $_{CP4}$EPSP synthase (Fig. 3*c*). This result suggested that the substrate-binding region of domain 1 in unliganded $_{Ab}$EPSP synthase exhibits structural aspects of closed $_{CP4}$EPSP synthase (Figs. 2*c* and 2*d*).

$_{Ab}$EPSP synthase residues Thr649–Arg661 formed an extended loop that connects the second β-strand to the second α-helix in subdomain VI (domain 1) and has been observed to undergo a conformational change as part of the open-to-closed transition upon S3P binding in $_{CP4}$EPSP and $_{Sp}$EPSP synthase (Funke *et al.*, 2006; Park *et al.*, 2004). This loop contains residues that are conserved in class II EPSP synthases, including several observed to directly participate in S3P and glyphosate binding (Lys353, Glu354 and Arg357 in $_{CP4}$EPSP synthase; Lys339, Glu340 and Arg343 in $_{Sp}$EPSP synthase; the analogous residues in $_{Ab}$EPSP synthase are Lys657, Glu658 and Arg661; Figs. 2*c* and 2*d*). In both $_{CP4}$EPSP and $_{Sp}$EPSP synthase this loop converted from an extended structure that is poorly defined by electron density to a compact stabilized conformation, including formation of the previously mentioned 3_{10}-helix, upon transition to the closed conformation. Moreover, both ligand-binding interactions plus interdomain interactions (*e.g.* an Arg128 guanidino–Val352 carbonyl hydrogen bond and an Arg132–Glu349 salt bridge in $_{CP4}$EPSP synthase) stabilize this region in the closed conformation.

The analogous unliganded $_{Ab}$EPSP synthase loop exhibited higher than average temperature factors, but was present in a conformation similar to that expected for the substrate-induced closed conformation, including the formation of the 3_{10}-helix. However, because the overall protein was in the open conformation this loop lacked stabilizing contacts with domain 1 residues or bound ligand. This behavior has previously been reported for unliganded $_{CP4}$EPSP synthase crystallized in the presence of the monovalent cations K^{+} or Rb^{+}. The pre-formation of the substrate-binding sites may be related to the catalytic activity enhancement observed for class II EPSP synthases in the presence of monovalent cations (Du *et al.*, 2000; Funke *et al.*, 2006). Crystallization of $_{Ab}$EPSP synthase occurred in the presence of NaCl and KBr, and this structural observation suggests that $_{Ab}$EPSP synthase activity will be also enhanced by monovalent cations. However, as in $_{CP4}$EPSP synthase, no specific cation-binding sites were observed in the crystal structure.

3.3. $_{Ab}$EPSP synthase is predicted to belong to the class II subfamily

The sequence and tertiary structure of $_{Ab}$EPSP synthase were analyzed to predict whether it belonged to the class I (glyphosate-sensitive) or the class II (glyphosate-resistant) subfamily, as it has not previously been classified. $_{CP4}$EPSP synthase is a prototypical class II EPSP synthase owing to its ability to withstand high concentrations of the inhibitor while maintaining high catalytic efficiency. Residue Ala100 of $_{CP4}$EPSP synthase, which is located in a short loop within subdomain IV (domain 2), has been identified as a key determinant of glyphosate resistance (Funke *et al.*, 2006). The C^{β} atom of Ala100 protrudes into the glyphosate-binding site, resulting in reduced glyphosate affinity while minimally affecting the binding of the smaller PEP molecule (Funke *et al.*, 2006; Eschenburg *et al.*, 2002). In contrast, $_{Ab}$EPSP synthase has a glycine (Gly407) at this position. Glycine, lacking a side chain, would not be expected to cause a steric clash with bound glyphosate. However, $_{CP4}$EPSP synthase is an outlier in the class II subfamily, as most members possess a glycine rather than an alanine at this position. Thus, the

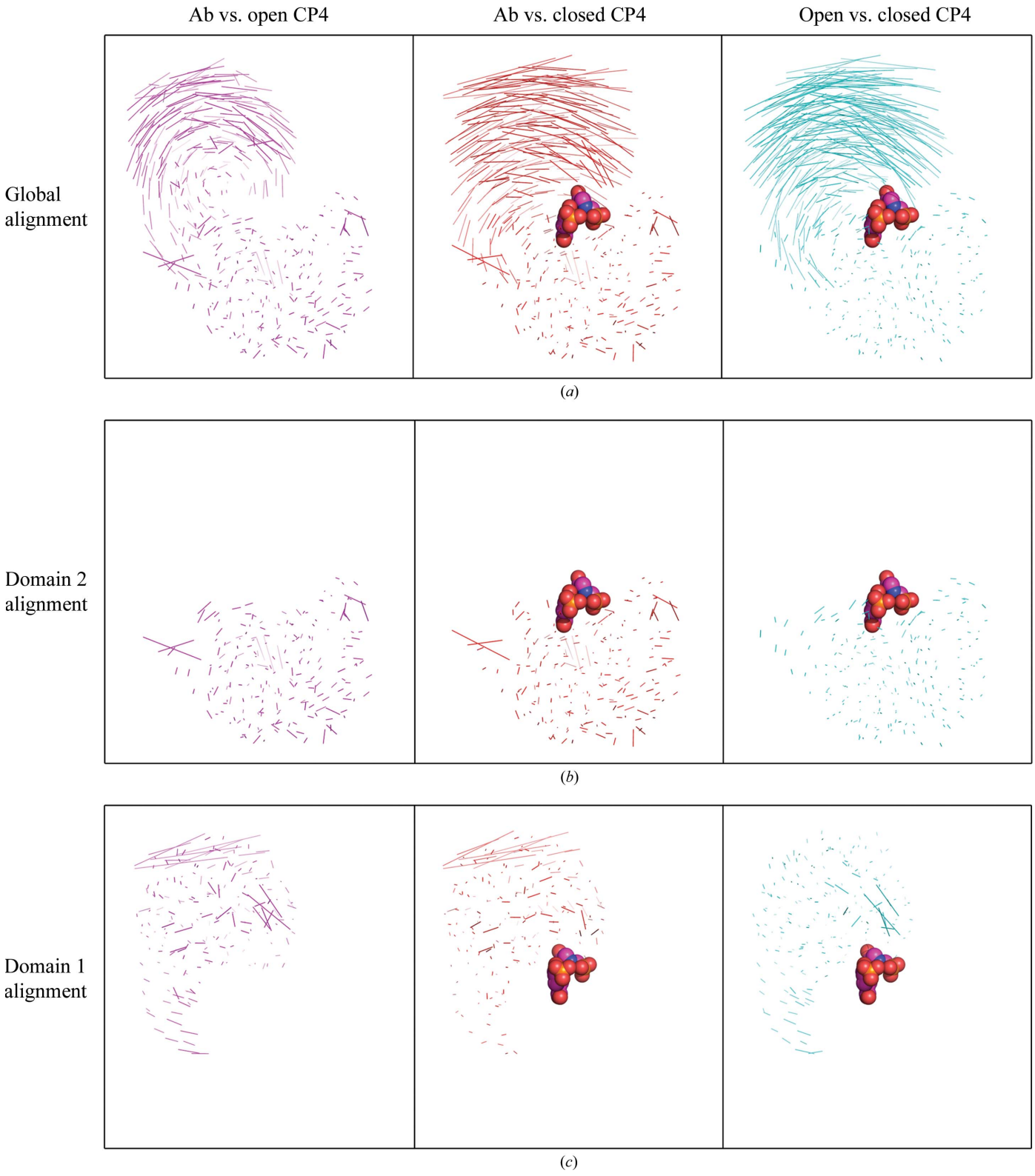

Figure 3
Displacements of paired atoms for superimposed EPSP synthase structures. The displayed lines connect atoms paired between superimposed proteins, providing a comparison of global and localized structural differences. Columns are labelled as follows: Ab vs. open CP4, superimposed open (unliganded) $_{Ab}$EPSP and $_{CP4}$EPSP (PDB entry 2gg4) synthases; Ab vs. closed CP4, superimposed open (unliganded) $_{Ab}$EPSP synthase and closed $_{CP4}$EPSP synthase–S3P–glyphosate complex (PDB entry 2gga); open vs. closed CP4, superimposed open and closed $_{CP4}$EPSP synthases (PDB entries 2gg4 and 2gga, respectively). (*a*) Global alignment: structural alignment over both domains to emphasize gross domain movements. (*b*) Domain 2: only domain 2 superimposed and displayed to emphasized differences localized within domain 2. (*c*) Domain 1 alignment: only domain 1 superimposed and displayed to emphasize differences localized within domain 1. SP3 and glyphosate are displayed when present in a structure included in the comparison. The protein orientation is identical to that in Fig. 2.

presence of this glycine is not a strong predictor of glyphosate sensitivity. Rather, the presence of Ala100 in $_{CP4}$EPSP synthase or other EPSP synthases serves as a marker of enhanced glyphosate resistance (Eschenburg *et al.*, 2002; Funke *et al.*, 2006; Sost & Amrhein, 1990).

Structure–function studies strongly support that glyphosate sensitivity is largely dictated by second-sphere residues near the overlapping PEP- and glyphosate-binding sites causing subtle changes in binding-site architecture rather than primarily owing to notable differences in residues directly contacting PEP or glyphosate (Eschenburg *et al.*, 2002; Funke *et al.*, 2009; Healy-Fried *et al.*, 2007; Priestman *et al.*, 2005; Sammons & Gaines, 2014). Several class-differentiating motifs have been reported (Funke *et al.*, 2009; Li *et al.*, 2009). Class I enzymes have a highly conserved motif corresponding to *E. coli* EPSP ($_{Ec}$EPSP) synthase residues ^{90}LFLGN AGTAM RPLAA^{104} (Fig. 4*a*; Funke *et al.*, 2009). Mutations within this conserved motif can confer glyphosate resistance (*e.g.* $_{Ec}$EPSP synthase G96A or the double mutant T97I/P101S; Eschenburg *et al.*, 2002; Funke *et al.*, 2009; Healy-Fried *et al.*, 2007). The $_{Ec}$EPSP synthase G96A mutant mimics the glyphosate-resistance determinant Ala100 in $_{CP4}$EPSP synthase. However, this $_{Ec}$EPSP synthase mutant significantly reduced the affinity for both glyphosate and PEP. Importantly, neither Thr97 nor Pro101 directly contact glyphosate, but the dual mutation shifted the position of Gly96 to interfere with glyphosate binding while minimally altering PEP utilization. $_{Ab}$EPSP synthase has a substantially different sequence (^{401}LYMGN SGTSM RLLSG^{415}) to that of the conserved class I motif. Moreover, this motif is not conserved in $_{CP4}$EPSP synthase and other class II EPSP synthases (Figs. 4*b* and 4*c*), suggesting that $_{Ab}$EPSP synthase does not belong to the glyphosate-sensitive class I.

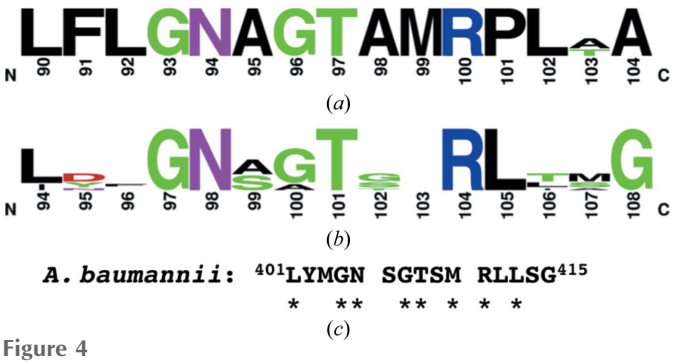

Figure 4
$_{Ab}$EPSP synthase lacks a motif conserved within class I (glyphosate-sensitive) EPSP synthases. (*a*) A logo representation of a motif adjacent to the PEP/glyphosate-binding site that is highly conserved within class I EPSP synthases (Funke *et al.*, 2009). The residue numbering is based upon the *E. coli* ortholog. (*b*) Logo representation of the corresponding region in class II EPSP synthases, with residue numbering based on the *Agrobacterium* sp. strain CP4 ortholog crystal structures. [The class II logo was constructed using EPSP synthase sequences from *Agrobacterium* sp. CP4 (Q0R4E4), *Pseudomonas* sp. PG2982 (P0A2Y4), *Achromobacter* sp. LBAA (P0A2Y5), *Pseudomonas stutzeri* A1501 (ABP79994), *Streptococcus pneumoniae* (Q9S400) and *Staphylococcus aureus* (Q05615).] (*c*) The sequence of the corresponding region in $_{Ab}$EPSP synthase, with asterisks indicating residues identical to the class I motif.

Class II EPSP synthases possess a conserved RPM*X*R motif that is required for both catalytic activity and glyphosate insensitivity. The leading arginine residue forms a salt bridge to the phosphate group of PEP (*e.g.* Arg128 of $_{CP4}$EPSP synthase; PDB entry 2gga; Funke *et al.*, 2006; Li *et al.*, 2009). This motif is present in $_{Ab}$EPSP synthase (^{435}RPMER^{439}), further supporting the classification of $_{Ab}$EPSP synthase as a class II (glyphosate-resistant) subfamily member. The non-conserved fourth position in this motif accommodates a variety of amino-acid types, including Gly, Asn, Asp, Arg and Lys (Li *et al.*, 2009). The glutamate residue present in $_{Ab}$EPSP synthase further expands the allowed repertoire of this variable position. The equivalent residues in class I enzymes display similarity at the N-terminus of the motif and become dissimilar towards the C-terminus (RP*hXX*, where *h* is a hydrophobic residue).

4. Conclusions

Antimicrobials effective against the ESKAPE pathogens, including *A. baumannii*, are urgently needed, especially those that employ new mechanisms of action. Several properties of $_{Ab}$EPSP synthase are appealing as an antimicrobial target, including the *in vivo* essentiality of both itself and other enzymes in the shikimate metabolic pathway and the lack of a human homolog. Furthermore, the effectiveness of glyphosate as an herbicide targeting EPSP synthases suggests that the family is druggable. The unliganded crystal structure of $_{Ab}$EPSP synthase was determined as part of its evaluation as an antimicrobial target. The $_{Ab}$EPSP synthase structure and sequence suggested that it belongs to the glyphosate-resistant class II subfamily. However, it is likely not to be as tolerant to high glyphosate concentrations as $_{CP4}$EPSP synthase owing to the presence of a glycine (Gly407) rather than an alanine at the PEP- and glyphosate-binding site. It was also predicted that monovalent cations enhance the catalytic activity of $_{Ab}$EPSP synthase, based upon the presence of a 3_{10}-helix in a key ligand-binding loop within subdomain VI in the unliganded state.

Previous research on EPSP synthases primarily focused on the overlapping PEP- and glyphosate-binding sites owing to the role of the enzyme as a commercially valuable herbicide target. Importantly, these efforts identified a number of natural and engineered glyphosate-resistant EPSP synthases. However, many of these engineered mutants were simultaneously catalytically less efficient. This observation suggests that a small-molecule antimicrobial designed to bind competitively with PEP may be subject to the development of resistant mutants, some of which may also exhibit decreased biofitness. The S3P binding site has been less explored as an inhibitor- or drug-binding site. It offers potential for the development of a multi-target therapeutic, as the S3P substrate shares chemical similarity with the substrates of other members, shikimate dehydrogenase and shikimate kinase, of the essential shikimate pathway (Hsu *et al.*, 2013), which could hold the promise of increased durability.

Therefore, next-stage studies in the assessment of $_{Ab}$EPSP are warranted.

Acknowledgements

This work was supported in part by a Telemedicine and Advance Technical Research Center (TATRC) Cooperative Agreement (W23RYX1055N607; TAR, LWS and TCU), an Interdisciplinary Grant from the University at Buffalo (TAR and TCU) and a VA Merit Review grant from the Department of Veterans Affairs (TAR). We wish to thank Ms Jessica Graham, Ms Changyi Ji, Mr Ritwik Nandagiri and Mr Hong Guo for assistance in $_{Ab}$EPSP synthase expression-vector preparation. The Ulp1 protease expression vector was a kind gift from Dr Christopher Lima (Sloan-Kettering Institute).

References

Abell, C. (1999). *Comprehensive Natural Products Chemistry*, edited by D. Barton, K. Nakanishi & O. Meth-Cohn, pp. 573–607. Oxford: Pergamon.

Adams, P. D. *et al.* (2010). *Acta Cryst.* D**66**, 213–221.

Adams, M. D., Goglin, K., Molyneaux, N., Hujer, K. M., Lavender, H., Jamison, J. J., MacDonald, I. J., Martin, K. M., Russo, T., Campagnari, A. A., Hujer, A. M., Bonomo, R. A. & Gill, S. R. (2008). *J. Bacteriol.* **190**, 8053–8064.

Afonine, P. V., Grosse-Kunstleve, R. W., Echols, N., Headd, J. J., Moriarty, N. W., Mustyakimov, M., Terwilliger, T. C., Urzhumtsev, A., Zwart, P. H. & Adams, P. D. (2012). *Acta Cryst.* D**68**, 352–367.

Bentley, R. & Haslam, E. (1990). *Crit. Rev. Biochem. Mol. Biol.* **25**, 307–384.

Boucher, H. W., Talbot, G. H., Benjamin, D. K. Jr, Bradley, J., Guidos, R. J., Jones, R. N., Murray, B. E., Bonomo, R. A. & Gilbert, D. (2013). *Clin. Infect. Dis.* **56**, 1685–1694.

Centers for Disease Control and Prevention (2013). *Antibiotic Resistance Threats in the United States, 2013*, pp. 59–60. http://www.cdc.gov/drugresistance/threat-report-2013. Atlanta: Centers for Disease Control and Prevention.

Coggins, J. R., Abell, C., Evans, L. B., Frederickson, M., Robinson, D. A., Roszak, A. W. & Lapthorn, A. P. (2003). *Biochem. Soc. Trans.* **31**, 548–552.

Crooks, G. E., Hon, G., Chandonia, J.-M. & Brenner, S. E. (2004). *Genome Res.* **14**, 1188–1190.

Du, W., Wallis, N. G., Mazzulla, M. J., Chalker, A. F., Zhang, L., Liu, W.-S., Kallender, H. & Payne, D. J. (2000). *Eur. J. Biochem.* **267**, 222–227.

Emsley, P., Lohkamp, B., Scott, W. G. & Cowtan, K. (2010). *Acta Cryst.* D**66**, 486–501.

Eschenburg, S., Healy, M. L., Priestman, M. A., Lushington, G. H. & Schönbrunn, E. (2002). *Planta*, **216**, 129–135.

Franz, J. E., Mao, M. K. & Sikorski, J. A. (1997). *Glyphosate: A Unique Global Herbicide*. Washington: American Chemical Society.

Funke, T., Han, H., Healy-Fried, M. L., Fischer, M. & Schönbrunn, E. (2006). *Proc. Natl Acad. Sci. USA*, **103**, 13010–13015.

Funke, T., Yang, Y., Han, H., Healy-Fried, M., Olesen, S., Becker, A. & Schönbrunn, E. (2009). *J. Biol. Chem.* **284**, 9854–9860.

Garnacho-Montero, J. & Amaya-Villar, R. (2010). *Curr. Opin. Infect. Dis.* **23**, 332–339.

Göttig, S., Gruber, T. M., Higgins, P. G., Wachsmuth, M., Seifert, H. & Kempf, V. A. (2014). *J. Antimicrob. Chemother.* **69**, 2578–2579.

Haslam, E. (1974). *The Shikimate Pathway*, edited by E. Haslam, pp. 128–185. London: Butterworth-Heinemann.

Healy-Fried, M. L., Funke, T., Priestman, M. A., Han, H. & Schonbrunn, E. (2007). *J. Biol. Chem.* **282**, 32949–32955.

Herrmann, K. M. & Weaver, L. M. (1999). *Annu. Rev. Plant Physiol. Plant Mol. Biol.* **50**, 473–503.

Hsu, K.-C., Cheng, W.-C., Chen, Y.-F., Wang, W.-C. & Yang, J.-M. (2013). *PLoS Comput. Biol.* **9**, e1003127.

Kim, B.-N., Peleg, A. Y., Lodise, T. P., Lipman, J., Li, J., Nation, R. & Paterson, D. L. (2009). *Lancet Infect. Dis.* **9**, 245–255.

Krissinel, E. (2015). *Nucleic Acids Res.* **43**, W314–W319.

Lee, H.-Y., Chen, C.-L., Wu, S.-R., Huang, C.-W. & Chiu, C.-H. (2014). *Crit. Care Med.* **42**, 1081–1088.

Levin, J. G. & Sprinson, D. B. (1964). *J. Biol. Chem.* **239**, 1142–1150.

Li, L., Lu, W., Han, Y., Ping, S., Zhang, W., Chen, M., Zhao, Z., Yan, Y., Jiang, Y. & Lin, M. (2009). *J. Biotechnol.* **144**, 330–336.

Luft, J. R., Collins, R. J., Fehrman, N. A., Lauricella, A. M., Veatch, C. K. & DeTitta, G. T. (2003). *J. Struct. Biol.* **142**, 170–179.

McConkey, G. A., Pinney, J. W., Westhead, D. R., Plueckhahn, K., Fitzpatrick, T. B., Macheroux, P. & Kappes, B. (2004). *Trends Parasitol.* **20**, 60–65.

Miethke, M. & Marahiel, M. A. (2007). *Microbiol. Mol. Biol. Rev.* **71**, 413–451.

Napier, B. A., Burd, E. M., Satola, S. W., Cagle, S. M., Ray, S. M., McGann, P., Pohl, J., Lesho, E. P. & Weiss, D. S. (2013). *MBio*, **4**, e00021-13.

Otwinowski, Z. & Minor, W. (1997). *Methods Enzymol.* **276**, 307–326.

Padgette, S. R., Kolacz, K. H., Delannay, X., Re, D. B., LaVallee, B. J., Tinius, C. N., Rhodes, W. K., Otero, Y. I., Barry, G. F., Eichholtz, D. A., Peschke, V. M., Nida, D. L., Taylor, N. B. & Kishore, G. M. (1995). *Crop Sci.* **35**, 1451–1461.

Park, H., Hilsenbeck, J. L., Kim, H. J., Shuttleworth, W. A., Park, Y. H., Evans, J. N., Kang, C. (2004). *Mol. Microbiol.* **51**, 963–971.

Paterson, D. L. & Harris, P. N. (2015). *Clin. Infect. Dis.* **61**, 155–156.

Perez, F., Hujer, A. M., Hujer, K. M., Decker, B. K., Rather, P. N. & Bonomo, R. A. (2007). *Antimicrob. Agents Chemother.* **51**, 3471–3484.

Priestman, M. A., Healy, M. L., Funke, T., Becker, A. & Schönbrunn, E. (2005). *FEBS Lett.* **579**, 5773–5780.

Rolain, J.-M., Diene, S. M., Kempf, M., Gimenez, G., Robert, C. & Raoult, D. (2013). *Antimicrob. Agents Chemother.* **57**, 592–596.

Russo, T. A., Luke, N. R., Beanan, J. M., Olson, R., Sauberan, S. L., MacDonald, U., Schultz, L. W., Umland, T. C. & Campagnari, A. A. (2010). *Infect. Immun.* **78**, 3993–4000.

Russo, T. A., MacDonald, U., Beanan, J. M., Olson, R., MacDonald, I. J., Sauberan, S. L., Luke, N. R., Schultz, L. W. & Umland, T. C. (2009). *J. Infect. Dis.* **199**, 513–521.

Sammons, R. D. & Gaines, T. A. (2014). *Pest Manag. Sci.* **70**, 1367–1377.

Schönbrunn, E., Eschenburg, S., Shuttleworth, W. A., Schloss, J. V., Amrhein, N., Evans, J. N. & Kabsch, W. (2001). *Proc. Natl Acad. Sci. USA*, **98**, 1376–1380.

Sost, D. & Amrhein, N. (1990). *Arch. Biochem. Biophys.* **282**, 433–436.

Spellberg, B. & Bonomo, R. A. (2014). *Crit. Care Med.* **42**, 1289–1291.

Stallings, W. C., Abdel-Meguid, S. S., Lim, L. W., Shieh, H.-S., Dayringer, H. E., Leimgruber, N. K., Stegeman, R. A., Anderson, K. S., Sikorski, J. A., Padgette, S. R. & Kishore, G. M. (1991). *Proc. Natl Acad. Sci. USA*, **88**, 5046–5050.

Sutton, K. A., Breen, J., MacDonald, U., Beanan, J. M., Olson, R., Russo, T. A., Schultz, L. W. & Umland, T. C. (2015). *Acta Cryst.* D**71**, 1736–1744.

Umland, T. C., Schultz, L. W., MacDonald, U., Beanan, J. M., Olson, R. & Russo, T. A. (2012). *MBio*, **3**, e00113-12.

Umland, T. C., Schultz, L. W. & Russo, T. A. (2014). *Future Microbiol.* **9**, 1113–1116.

Vagin, A. & Teplyakov, A. (2010). *Acta Cryst.* D**66**, 22–25.

Villar, M., Cano, M. E., Gato, E., Garnacho-Montero, J., Cisneros, J. M., Ruíz de Alegría, C., Fernández-Cuenca, F., Martínez-Martínez, L., Vila, J., Pascual, A., Tomás, M., Bou, G. & Rodríguez-Baño, J. (2014). *Medicine*, **93**, 202–210.